Lanthanoid-containing anilato complexes and lattices

Subjects: Others

Contributor: Carlos Gomez Garcia

Coordination polymers (CPS) and metal organic frameworks (MOFs) with lanthanide compounds (LN) have attracted more and more attention in the past decade, because they may exhibit gas and solvent exchange and adsorption / absorption, and exhibit interesting magnetic and luminescent properties, so they can be used to prepare optical and magnetic sensors for gases.

Keywords: luminescence ; single-ion magnet ; single-molecule m

1. Introduction

The field of coordination polymers (CPs) and metal organic frameworks (MOFs) with lanthanoids (Ln) is gaining interest in this decade since they may show gas and solvent exchange and adsorption/absorption and present interesting magnetic and luminescent properties and can, therefore, be used to prepare optical and magnetic sensors of gases, contaminants and different chemical species [1][2][3].

Among the many different ligands that can be used to construct these CPs and MOFs, anilato-type ligands (3,6-disubstituted-2,5-dihydroxy-1,4-benzoquinone dianion = $C_6O_4X_2^{2-}$, Scheme 1a) are becoming very popular since these ligands present some interesting properties: (i) They show different coordination modes as: monodentate (*1kO*), bidentate (*1k^{2}O,O'*), bis-bidentate (*1k^{2}O,O';2k^{2}O'',O'''*), monodentate-bidentate (*1kO;2k^{2}O',O''*) or even more complex coordination modes such as (*1k^{2}O,O';2k^{2}O'',O''';3kO''*) (Scheme 1c–f) [4][5]. (ii) They can act as linear bridges connecting two metal atoms (Scheme 1a) to generate many different coordination polymers [4]. (iii) They couple (antiferro)magnetically the metal centers when they are transition metal ions and the coupling can be modulated by changing X [6]. (iv) They provide a good magnetic isolation when bridging lanthanoids (as a result of the negligible overlap with the 4f orbitals), giving rise to single-molecule and single-ion magnet behaviours (SMM and SIM). (v) They can be reduced by one or two electrons to their semiquinone and cathecolate forms (Scheme 1b), resulting in an increase in the magnetic coupling and ordering temperatures [7]. (vi) They are topologically equivalent to the well-known oxalato ligand ($C_2O_4^{2-}$) and they are able to form similar monomeric complexes [8][9] as well as extended 1D, 2D and 3D lattices although with much larger cavities and channels [10][11].

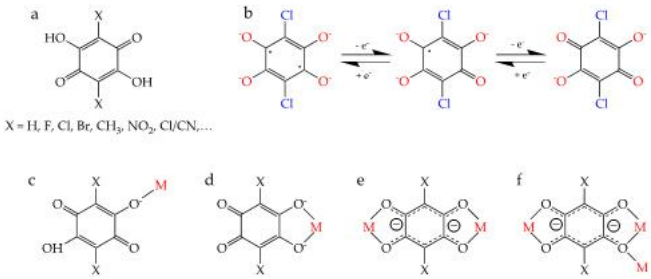

Scheme 1. (**a**) The 3,6-disubstituted anilato derivatives ($H_2C_6O_4X_2$). (**b**) Reduced forms of the chloranilato ligand (right): semiquinone (center) and cathecolate (left). (**c**–**f**) Different coordination modes of the anilato ligands. (**c**) monodentate (*1kO*), (**d**) bidentate (*1k^{2}O,O'*), (**e**) bis-bidentate (*1k^{2}O,O';2k^{2}O'',O'''*) and **(f)** bis-bidentate-monodentate (*1k^{2}O,O';2k^{2}O'',O''';3kO''*).

Although anilato and its derivatives (Scheme 1a) have been combined with transition metals since the 1950s [12], the use of lanthanoids with anilato ligands was not developed until the 21st century. Surprisingly, there are only three reports in the 20th century. The first one, published in 1983 by Raymon *et al*. [13] describes a compound with Pr(III) and chloranilate (X = Cl). The second one, published in 1987 by Robl *et al*. [14] presents a couple of Y(III) compounds with chloranilate and bromanilate (X = Br). The third report was published in 1996 by Robson, Abrahams *et al*. [15] and contains a Ce(III) compound with $dhbq^{2-}$ (X = H).

The first complete and systematic study was performed by Robson, Abrahams *et al.* in 2002 [16]. In this seminal article, the authors prepared and structurally characterized a total of 19 Ln-anilato compounds (and one with Sc) using $dhbq^{2-}$ (X = H) and chloranilato (X = Cl). Since then, almost 150 Ln-anilato compounds have been prepared, as we will show in this review.

The structures and properties of homometallic coordination polymers prepared with anilato ligands and transition metals (and even p- and s-block metals) were revised in a very complete study in 2002 by Kitagawa and Kawata. More recently, in 2017, Mercuri *et al.* [17] performed a complete revision, focusing on the magnetic and conducting properties, of homo- and heterometallic complexes and coordination polymers with anilato and transition metals. Finally, we have very recently revised the heterometallic anilato-based 2D and 3D lattices with transition metals [18].

Surprisingly, as far as we know, no revision of the almost 150 prepared lanthanoid-anilato compounds has been published to date. Therefore, here we revise all the structurally characterized Ln-anilato compounds. We will show the different anilato-type ligands used (Scheme 1a) and their magnetic and luminescent properties. We will also show the gas and solvent adsorption/absorption and the solvent exchange capacity of some of them as well as the attempts to reduce the anilato bridge in some dimers. Finally, we will show the delamination of some of the layered lattices into thin films with promising properties.

This review is organized into seven different sections: In Section 1, we introduce the anilato-type ligands and their properties as well as their capacity to coordinate in a bis-bidentate way and to act as bridges connecting lanthanoid ions in coordination complexes and polymers. In Section 2, we will show and describe all the reported structures: (i) discrete monomers, dimers and tetramers; (ii) zigzag and ladder-type chains; (iii) hexagonal, rectangular and square layers; and (iv) 3D structures. In Section 3, we will show the magnetic properties of some of these compounds, focusing on their (in most cases, field-induced) single-molecule magnet (SMM) and single-ion magnet (SIM) behaviours. In Section 4, we will show their optical properties, including luminescence in the visible and NIR regions. In Section 5, we will show the porosity, gas and solvent adsorption/absorption and solvent exchange capacity of some of the layered Ln-anilato materials. In Section 6, we will show their redox properties and, finally, in Section 7, we will show how it is possible to easily delaminate some of the layered compounds to prepare thin films with nanometric thickness.

2. Structural classification

Discrete (0D) Complexes

There are 33 reported discrete complexes containing lanthanoids and anilato ligands. There are thirty dimers (**2**-**31**), two monomers (**1** and **33**) and one tetramer (**32**).

One Dimensional (1D) Lattices

There are only two known 1D polymers containing Ln and anilato-type ligands: $[Lu(C_6O_4Cl_2)(H_2O)_4][Lu(C_6O_4Cl_2)_2(H_2O)_4]\cdot\approx 4H_2O$ (**33**) [19] and $[Er_2(C_6O_4Cl_2)_3(hmpa)(H_2O)_3]\cdot H_2O$ (**34**) (hmpa = hexamethylphosphoramide) [20].

Two-Dimensional (2D) Lattices

Two-dimensional lattices are, by far, the most common ones in the Ln-anilato family of compounds, with more than one hundred known examples. In order to rationalize these 2D lattices, we have classified them according to their topology and shape of the rings forming the layers. The most recurrent ones are the hexagonal 3,6-gon and square 4,4-gon topologies.

The 3,6-gon topology is, by far, the most abundant one, with more than 90 reported examples. In this topology, each Ln(III) is connected to three other Ln(III) ions through anilato bridges giving rise to regular (Figure 1a) or distorted (Figure 1b) hexagonal rings with the typical honey comb hexagonal structure. In some of these lattices the hexagons are so distorted that they look like rectangles (with two Ln-Ln-Ln angles close to 180°). These rectangular six-membered rings may adopt a brick-wall structure (Figure 1c) or a herringbone one (Figure 1d).

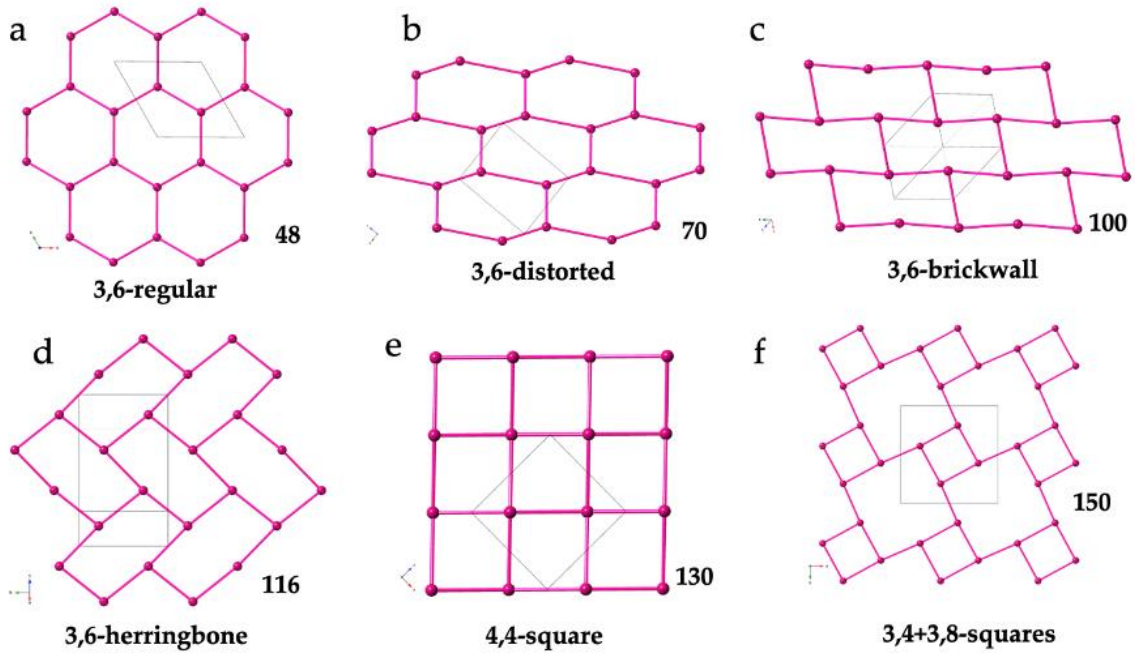

Figure 1. Schematic views of the different 2D lattices found in Ln-anilato compounds: (**a**) View of the (3,6) lattice with regular hexagons in **48**. (**b**) View of the (3,6) lattice with distorted hexagons in **70**. (**c**) View of the (3,6) lattice with rectangular rings in a brick-wall structure in **100**. (**d**) View of the (3,6) lattice with rectangular rings in a herringbone structure in **116**. (**e**) View of the (4,4) lattice in **130**. (**f**) View of the (3,4)+(3,8) lattice in **150**. Only the Ln(III) ions are displayed for clarity. The pink bonds represent the anilato bridges.

Three Dimensional (3D) Lattices

There are only seven reported 3D Ln-anilato compounds, all with chloranilato and six of them reported in 2019. Except compounds **156** and **157**, they all show the well-known adamantane lattice, although with large distortions.

3. Magnetic Properties

Single-Molecule and Single-Ion Magnets

Most of the magnetically characterized Ln-anilato compounds show the expected magnetic properties of isolated Ln(III) ions with the corresponding decrease in the $\chi_m T$ product when the temperature is decreased as a result of the depopulation of the excited levels that appear due to the ligand field. This behaviour confirms the absence of noticeable magnetic interactions through the anilato bridges when connecting Ln(III) ions. In fact, only when connecting transition metals, anilato bridges show weak antiferromagnetic interactions (that can be modulated by the X group). Although this lack of magnetic interactions may appear as a disadvantage from the magnetic point of view, the good magnetic isolation provided by the anilato ligands precludes the fast relaxation of the magnetization and allows the synthesis of Ln-anilato complexes and coordination polymers behaving as single-molecule magnets (SMMs) and single-ion magnets (SIMs) with slow relaxation of the magnetization. SMMs and SIMs are attracting many interest recently since they present memory effects and quantum phenomena that may find applications in data storage, quantum computing and spintronics. SMMs and SIMs retain their spin orientation and show a slow relaxation of the magnetization at low temperatures that may follow different mechanisms such as: (i) Orbach (O), (ii) Raman (R), (iii) direct (D) and (iv) quantum tunnelling (QT). The O, R and D mechanisms are temperature dependent and the D and QT mechanisms are field dependent. Usually, when several mechanisms are operative, the relaxation time is determined by the faster process and, thus, QT is operative at low temperatures (when no DC field is applied), whereas Orbach mechanism is the dominant one at high temperatures. In some cases, the application of a DC field (usually below 3000 Oe) suppress the fast relaxation through the QT mechanism. In these compounds, called field-induced-SMM of field induced-SIM (FI-SMM or FI-SIM), the application of a DC field is required to observe the slow relaxation of the magnetization and the direct mechanism may contribute to the relaxation of the magnetization. The equation used to reproduce the relaxation rate (the inverse of the relaxation times, τ) as a function of the temperature and/or DC field includes the O, R, D and QT mechanisms as follow :

$$\tau^{-1} = \tau_0^{-1} exp\left(\frac{-U_{eff}}{k_B T}\right) + CT^n + AH^2T + \tau_{QTM}^{-1}. \quad (1)$$

Surprisingly, the possibility to prepare Ln-anilato-based SMMs and SIMs has not been exploited until very recently (Table 28). Thus, the first Ln-anilato complexes showing SMM behaviour were reported in 2017 by Boskovic *et al.* in two closely related Dy(III) dimers $[(Tp)_2Dy_2(C_6O_4Cl_2)]\cdot 2CH_2Cl_2$ (**4**) and $[(Tp)_2Dy_2(C_6O_4(CH_3)_2)]\cdot 1.1CH_2Cl_2$ (**4′**) (Tp^- = hydrotris(pyrazolyl)borate = $HB(pz)_3$) [20]. Although only the structure of compound **4** was reported, compound **4′** is isostructural to the Y analogue $[(Tp)_2Y_2(C_6O_4(CH_3)_2)]\cdot 1.2CH_2Cl_2$ (**11**) . Compound **4′** shows an almost temperature

independent slow relaxation of the magnetization that follows a quantum tunnelling mechanism when no DC field is applied at low temperatures and when a DC field of 1600 Oe is applied, both compounds (**4** and **4′**) show slow relaxation of the magnetizations with an Orbach relaxation mechanism for **4′** with U_{eff} = 47 K and Orbach and Raman mechanisms for **4** with U_{eff} = 24 K.

Compound $[(Tp)_2Dy_2(C_6O_4Cl_2)]\cdot 2CH_2Cl_2$ (**4**) was almost simultaneously reported twice more (compounds **5** and **6** in Table 28) by Slageren *et al.* and by Ishikawa *et al.*. Both reports confirm the FI-SMM behaviour of compound **4** and complete the magnetic studies with different applied DC fields and temperature ranges. Furthermore, Slageren *et al.* showed that when the chloranilato bridge is chemically reduced using cobaltocene, the Dy and Tb dimers (**4** and **24**, respectively) behave as SMM even with no applied DC field. Slageren also showed that when a DC field of 1000 Oe is applied, the reduced Dy derivative shows two different relaxation processes. The energy barriers obtained by Slageren *et al.*, even when the choranilato bridge was reduced, are similar to those obtained by Boskovic *et al.* (Table 28). The third study, made by Ishikawa *et al.*, was performed with a DC field of 950 Oe and also showed a similar energy barrier for the high temperature data although now the relaxation times was fit to a model including only Raman and Direct mechanisms. In this study, Ishikawa *et al.* also reported the monomer $[Co(Cp)_2][Dy(Tp)_2(C_6O_4Cl_2)]$ (**1**), that also behaves as a FI-SMM with an energy barrier of 49.4 K when a DC field of 1500 Oe is applied. Under this DC field, the relaxation of the magnetization of compound **1** follows Raman and Direct mechanisms .

Boskovic *et al.* reported in 2019 a similar dimer to compound **4** but prepared with bromanilato instead of chloranilato: $[(Tp)_2Dy_2(C_6O_4Br_2)]$ (**18**). Compound **18** is also a FI-SMM and presents a low energy barrier of 7 K when a DC field of 390 Oe is applied. As observed in dimer **4**, when the bromanilato bridge in dimer **18** is reduced, the compound behaves as a SMM with zero applied DC field. The reduced dimer **18** also shows low energy barriers of 10.4 and 10.6 K for DC fields of 0 and 380 Oe, respectively. In all cases, the relaxation of the magnetization follows Orbach, Raman and direct mechanisms .

In addition, in 2019, Ishikawa *et al.* reported the Er and Yb derivatives with chloranilato (compounds **22** and **29**, respectively, Table 28). Both compounds behave as FI-SMM and show energy barriers of 25.9 and 22.3 K, respectively, when a DC field of 1000 Oe is applied. In both cases, the relaxation times can be very well reproduced using Orbach and Raman mechanisms .

As can be seen in Table 28, all the above-mentioned SMM and FI-SMM complexes contain the coligand (Tp^- = hydrotris(pyrazolyl)borate = $HB(pz)_3$). The only reported dimer with SMM behaviour without the Tp^- coligand is compound $[Eu_{1.96}Dy_{0.04}(C_6O_4(CN)Cl)_3(H_2O)_{10}]\cdot 6H_2O$ (**31**) . This dimer shows a zigzag structure and contains a bridging chlorocyananilato ligand. Compound **31** is also the only doped dimer with SMM behaviour (contains Eu doped with 2% of Dy) and is also the only Ln-anilato dimer showing SMM without applying a DC field or reducing the bridging anilato ligand. This compound presents an energy barrier of 25.3 K and the relaxation of the magnetization could be fit to an Orbach and Direct mechanisms, although in this case, the frequency maxima appear at high frequencies and could not be observed.

Besides these discrete complexes (nine dimers and one monomer, Table 28), there are also six Ln-anilato 2D lattices showing FI-SMM or even SMM (in one case). Two of these six 2D lattices are isostructural 4,4-nets showing FI-SMM behaviour: $(NEt_4)[Dy(C_6O_4Cl_2)_2]$ (**135**) and $(NEt_4)[Gd(C_6O_4Cl_2)_2]$ (**136**). In both cases, the measurements were performed with a DC field of 1000 Oe, although no analysis of the relaxation mechanisms nor the energy barrier was reported . The observation of slow relaxation in compound **136** is very surprising since Gd(III) is an isotropic ion and is very unusual to observe SMM or FI-SMM behaviour in Gd(III) complexes . The exact mechanism to explain this unusual behaviour is not clear yet.

The four remaining 2D lattices showing slow relaxation of the magnetization are 3,6-networks (Table 28). Three of them contain Dy(III) and bromanilato: $[Dy_2(C_6O_4Br_2)_3(H_2O)_6]\cdot 8H_2O$ (**80**) , $[Dy_2(C_6O_4Br_2)_3(dmso)_4]\cdot 2dmso\cdot 2H_2O$ (**83**) and $[Dy_2(C_6O_4Br_2)_3(dmf)_6]$ (**125**), whereas the fourth one contains Eu doped with Dy: $[Dy_{0.04}Eu_{1.96}(C_6O_4Br_2)_3(dmso)_6]\cdot 2dmso$ (**123**). Compounds **80**, **83** and **125** are three closely related compounds that, in fact, show reversible interconversion upon solvent exchange (see below). Compounds **80** and **83** show distorted hexagonal 2D lattices whereas compound **125** shows a rectangular herringbone 2D structure. Compounds **80** and **83** show slow relaxation of the magnetization under a DC field of 1000 Oe (Figure 2a), with energy barriers of 9.6 and 22.8 K, respectively (Figure 2b).

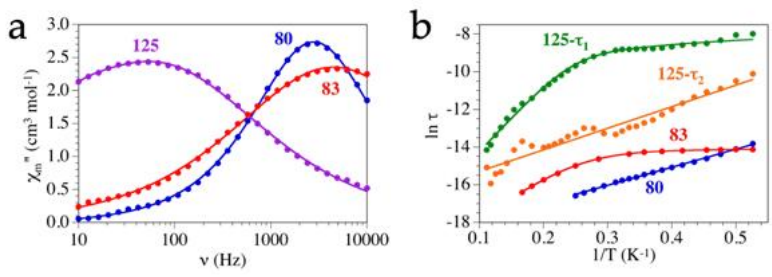

Figure 2. (**a**) Frequency dependence of χ_m" for compounds **80**, **83** and **125** at 1.9 K with a DC field of 1000 Oe. Solid lines are the fit to the Debye model with one (in **80** and **83**) or two (in **125**) relaxation processes. (**b**) Arrhenius plot with the relaxation time for compounds **80**, **83** and **125** with a DC field of 1000 Oe. Solid lines are the fit to the general model with

Orbach mechanism in **80** and the fast process (τ_2) in **125**; Orbach and direct mechanisms in the slow process (τ_1) in **125** and Orbach, direct and quantum tunnelling in **83**.

The relaxation of the magnetization follows an Orbach mechanism in compound **80**, whereas in compound **83** it follows Orbach, direct and quantum tunnelling mechanisms. Since both compounds show the same structure, Ln(III) ion and ligand, we can attribute these differences to the changes in the coordination geometry of the Dy(III) ions (TCTPR-9 in **80** *vs*. TDD-8 in **83**). These changes in the coordination number and geometry are due to the different sizes of the coligands (H_2O in **80** *vs*. dmso in **83**). Despite showing a different structure, compound **125** is closely related to compounds **80** and **83** (the only difference is that it contains dmf as coligand, instead of H_2O or dmso). Compound **125** also shows slow relaxation of the magnetization when a DC field of 1000 Oe is applied (Figure 2a), although now there are two different relaxation processes: (i) a slow relaxation process (SR) with an energy barrier of 36 K and a relaxation following Orbach and direct mechanisms and (ii) a fast relaxation (FR) process with an energy barrier of 11.4 K that relaxes following an Orbach mechanism (Figure 2b). Finally, compound **123** is the only 2D lattice showing slow relaxation of the magnetization with zero applied DC field. This compound shows an energy barrier of 40.9 K.

Table 1. Ln-anilato compounds with slow relaxation of the magnetization.

#	CCDC	Structure	Ln	X	Geometry[a]	A^+	L [b]	H (Oe)	U_{eff} (K)	Rel. Mec. [c]	Reference
1	PIQFUT	Mon.	Dy	Cl	SAPR-8	–	Tp^-	1500	49.4	R/D	[21]
4	DEKTOF	Dimer	Dy	Cl	TDD-8	–	Tp^-	1600	24	O/R	[22]
4′	-	Dimer	Dy	CH_3	TDD-8	–	Tp^-	1600	47	O	[22]
								1000	39	O	
5	DEKTOF01	Dimer	Dy	Cl	TDD-8	–	Tp^-	1000	31 [e]	O	[23]
								0	SMM [e]	O	
6	DEKTOF02	Dimer	Dy	Cl	TDD-8	–	Tp^-	950	44.7	R/D	[21]
								390	7	O/R/D	
18	JOQSEQ	Dimer	Dy	Br	TDD-8	–	Tp^-	0	10.4[e]	O/R/D	[24]
								380	10.6[e]	O/R/D	
22	KOZBEJ	Dimer	Er	Cl	TDD-8	–	Tp^-	1000	25.9	O/R	[25]
24	LEPNIG	Dimer	Tb	Cl	TDD-8	–	Tp^-	0	SMM[e]	–	[23]
29	OBIBEH01	Dimer	Yb	Cl	TDD-8	–	Tp^-	1000	22.3	O/R	[25]
31	NOQGEI	Dimer-zz	Eu/Dy [d]	Cl/CN	CSAPR-9	–	H_2O	0	25.3	O/D	[26]
80	1565279	2D-hex	Dy	Br	TCTPR-9	–	H_2O	1000	9.6	O	[27][28]
83	NIDFUE	2D-hex	Dy	Br	TDD-8	–	dmso	1000	22.8	O/D/QT	[29][28]
123	NOQBON	2D-herr	Eu/Dy [d]	Br	CSAPR-9	–	dmso	0	40.9	O/D	[26]
125	LUTROK	2D-herr	Dy	Br	CSAPR-9	–	dmf	1000	11.4 (FR) 36 (SR)	O O/D	[28]

135	QOFCEW	2D-4,4	Dy	Cl	SAPR-8	NEt_4^+	–	SMM	–	–	[30]
136	QOFNAD	2D-4,4	Gd	Cl	SAPR-8	NEt_4^+	–	SMM	–	–	[30]

([a]) The geometry was determined with the program SHAPE [29–36]. SAPR-8 = square antiprism, TDD-8 = triangular dodecahedron, CSAPR-9 = capped square antiprism; ([b]) Tp^- = $HB(pz)_3^-$ = hydrotris(pyrazolyl)borate, dmso = dimthylsulfoxide, dmf = dimethylformamide; ([c]) relaxation mechanism of the magnetization: O = Orbach, R = Raman, QT = quantum tunnelling, D = direct ([d]) Eu (98%)/Dy (2%); ([e]) data with the anilato bridge reduced.

3. Optical Properties

Besides magnetic properties, all these Ln-anilato compounds may also show interesting optical properties, such as luminescence, very common in many Ln-containing compounds [66]. Furthermore, some anilato ligands such as chlorocyananilato and nitranilato, may also show luminescence in solid state [31] and in solution [32][33], even when they are not coordinated. Table 29 shows all the structurally characterized Ln-anilato compounds showing luminescence with the corresponding ligand- and lanthanoid-based emission bands.

The first luminescence study on a Ln-anilato compound (and the only one with chloranilato) dates back to 2004 when Kaizaki *et al.* performed a study of the Yb(III) dimer: $[(YbTp)_2(C_6O_4Cl_2)]\cdot 2CH_2Cl_2$ (**28**). This compound shows a strong 4f-4f emission at *ca.* 1000 nm attributed to ligand-to-metal energy transfer from the triplet state of the chloranilato ligand to the excited 4f state of the Yb(III) ion . The strong absorption band at 560 nm observed in this compound was attributed to the chloranilato ligand. In contrast, the analogue dimers with Tb(III) or Eu(III) did not show any emission, suggesting the presence of a back-transfer from the Ln(III) ions to the chloranilato ligand.

The other dimers showing luminescence, $[Ln_2(C_6O_4(NO_2))_3(H_2O)_{10}]\cdot 6H_2O$ with Ln = Gd (**13**), Tb (**14**), Dy (**15**), Ho (**16**) and Sm (**17**) were reported in 2016. These dimers show the emission of the nitranilato ligand, centered at *ca.* 590 nm. In contrast to compounds **13**-**15** and **17**, where the anilato ligand does not sensitize the emission of the Ln(III) ions, in compound **16** there are two emission bands from the Ho(III) ions at 531 and 643 nm, attributed to the $^5F_4$ ® $^5I_8$ and $^5F_5$ ® $^5I_8$ transitions, respectively. Besides dimers, luminescence has also been very recently observed in some 2D Ln-anilato lattices. The first observation of luminescence in 2D lattices was reported in a chlorocyananilato lattice with Yb(III): $[Yb_2(C_6O_4(CN)Cl)_3(dmso)_4]\cdot 2H_2O$ (**87**) [46]. This compound shows the emission of the chlorocyananilato ligand at around 700 nm (Figure 3a), with a red shift of *ca.* 25 nm when compared with the free ligand in the solid $K_2(C_6O_4(CN)Cl)$ salt. Besides the ligand emission, compound **87** shows the typical emission in the NIR, at *ca.* 980 nm, corresponding to the $^2F_{5/2}$ ® $^2F_{7/2}$ transition of the Yb(III) ion (Figure 3b) . The related 2D lattices $[Pr_2(C_6O_4(CN)Cl)_3(dmso)_6]$ (**104**) and $[Pr_2(C_6O_4(CN)Cl)_3(dmf)_6]$ (**126**) also show the ligand emission at *ca.* 700 and 680 nm, respectively (although much weaker in **104**), but no emission from the Ln(III) ions could be observed.

Table 2. Ln-anilato complexes and lattices with anilato-based and/or Ln-based luminescence.

#	CCDC	Structure	Ln	X	Anilato (nm)	Ln(III) (nm)	Reference
13	EDEZAR	Dimer	Gd	NO_2	≈590	–	[23]
14	EDEZEV	Dimer	Tb	NO_2	≈590	–	[23]
15	EDEZIZ	Dimer	Dy	NO_2	≈590	–	[23]
16	EDEZOF	Dimer	Ho	NO_2	596	531, 643	[23]
17	EDEZUL	Dimer	Sm	NO_2	≈590	–	[23]
28	OBIBEH	Dimer	Yb	Cl	560	≈1000	[26]
53	XIKNOX	2D-hex	Nd	Cl/CN	≈650 ≈460 [a] 680–720 [b]	900, 1070, 1350	[34]

54	XIKPAL	2D-hex	Er	Cl/CN	≈650 ≈460 [a] 680–720 [b]	≈1550	[34]
80	1565279	2D-hex	Dy	Br	–	≈500	[35]
83	NIDFUE	2D-hex	Dy	Br	–	≈500	[35]
87	DIFLUC	Distorted 2D-hex	Yb	Cl/CN	≈700	980	[36]
88	POMTUJ	Distorted 2D-hex	Yb	Cl/CN	–	980	[37]
89	POMVAR	Distorted 2D-hex	Yb/Er	Cl/CN	–	980 1530	[37]
104	DIFLOW	2D-brick wall	Pr	Cl/CN	≈680	–	[36]
111	QOVJUJ	2D-brick wall	Yb	Cl/CN	650–900	≈1000	[38]
112	QOVJOD	2D-brick wall	Yb	Cl/CN	650–900	≈1000	[38]
125	LUTROK	2D-herr	Dy	Br	–	≈500	[35]
126	DIFLIQ	2D-herringbone	Pr	Cl/CN	≈680	–	[36]
127	XIKNUD	2D-herringbone	Yb	Cl/CN	≈650 ≈460 [a] 680–720 [b]	≈980	[34]
149	POMVIZ	2D-(3,4)+(3,8)	Er	Cl/CN	710	1530	[37]

([a]) Nanosheets suspension; ([b]) drop-casted nanosheets.

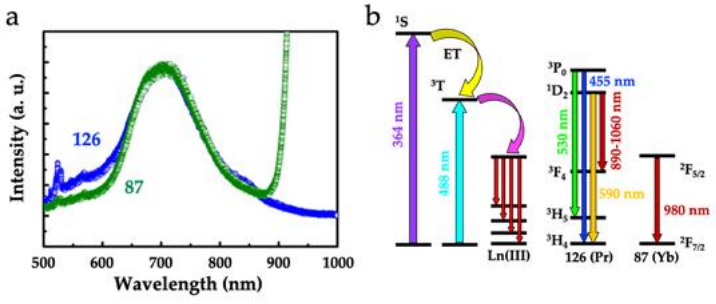

Figure 3. (**a**) Emission spectra of compounds **87** and **126** with an excitation wavelength of 364 nm. (**b**) Energy diagram with the main energy transfer and sensitization pathways in compounds **87** and **126**.

A recent study by Mercuri *et al.* of two related series, also with the ligand chlorocyananilato and dmso as solvent, formulated as $[Ln_2(C_6O_4(CN)Cl)_3(dmso)_4]\cdot dmso$, with Ln = Yb (**88**), Yb/Er (**89**) and $[Er_2(C_6O_4(CN)Cl)_3(dmso)_6]$ (**149**), showed similar results, further confirming the antenna effect of the chlorocyananilato ligand and the Ln-based emission in the NIR region. Thus, compounds **88** and **89** show an emission band at 980 nm, corresponding to the $^2F_{5/2}$ ® $^2F_{7/2}$ transition in the Yb(III) ions and compounds **89** and **149** show an emission band at 1530 nm, corresponding to the $^4I_{13/2}$ ® $^4I_{15/2}$ transition in the Er(III) ions. These compounds show high quantum yields of 15.6 % for the Yb(III) compound and 0.16 % for the Er(III) one, the highest reported for coordination compounds to date. Remarkably, these properties are retained in dmso solutions and in drop-casted films.

A very interesting report also by Mercuri *et al.* showed NIR emission in a family of three 2D lattices formulated as $[Ln_2(C_6O_4(CN)Cl)_3(dmf)_6]\cdot G$ with Ln/G = Nd/$2CH_2Cl_2$ (**53**), Er/$2CH_2Cl_2$ (**54**) and Yb/- (**127**). These layered compounds show the emission of the chlorocyananilato ligand at around 650 nm (with a red shift of *ca.* 50 nm when compared with the free ligand in the solid $KH(C_6O_4(CN)Cl)$ salt). Besides the ligand emission, the three compounds show the Ln(III) emission at *ca.* 900, 1070 and 1350 nm in **53**, *ca.* 1550 nm in **54** and *ca.* 980 nm in **127**, showing the antenna effect of the chlorocyananilato ligand. The measurements performed on suspensions of nanosheets of these compounds show that the emission of the Ln(III) ions are similar to those of the crystals but the ligand emission appears blue-shifted at *ca.* 460 nm, close to the value observed for the free ligand in dilute solution. When these nanosheets are drop-casted, the Ln(III) emission remains unchanged but the ligand emission appears at *ca.* 680-720 nm, close to the value observed in the crystals.

A similar study has very recently been performed by the same team on two original Ln-anilato 2D lattices including additional coligands such as the dianion of 2,5-dihydroxybenzene-1,4-dicarboxylic acid (H_2dobdc): $[Yb_4(C_6O_4(CN)Cl)_5(dobdc)(dmso)_{10}]\cdot 2dmso$ (**111**) and the dianion of 2,3,5,6-tetrafluorobenzene-1,4-dicarboxylic acid (H_2F_4bdc): $[Yb_2(C_6O_4(CN)Cl)_2(F_4bdc)(dmso)_6]$ (**112**). These two compounds show a very broad emission from *ca.* 650 nm to more than 900 nm attributed to the chlorocyananilato ligand together with a much stronger emission at *ca.* 1000 nm from the Yb(III) ions, showing once more the antenna effect of the ligand. Studies performed on nanosheets of compounds **111** and **112** show similar photoluminescence spectra although with much weaker signals.

Finally, luminescence has also been reported in three related 2D latices formulated as $[Dy_2(C_6O_4Br_2)_3(H_2O)_6]\cdot 8H_2O$ (**80**), $[Dy_2(C_6O_4Br_2)_3(dmso)_4]\cdot 2dmso\cdot 2H_2O$ (**83**) and $[Dy_2(C_6O_4Br_2)_3(dmf)_6]$ (**125**) that can be easily interconverted by solvent exchange and that also show FI-SMM behaviour (see above). These three compounds show an increase in the emission of the Dy(III) ion when changing the solvent from dmf (where the emission is almost completely quenched) to H_2O and dmso.

4. Gas/Solvent Adsorption/Absorption and Solvent Exchange

Very recently, gas and solvent adsorption and even solvent exchange have been reported in some Ln-anilato compounds (Table 30). The first observation of gas adsorption in a Ln-anilato compound was reported in the series $[Ln_2(dhbq)_3(H_2O)_6]\cdot 18H_2O$ with Ln(III) = Ho (**35**), La (**36**), Gd (**37**), Yb (**38**), Lu (**39**), Y (**40**), Er (**41**), Ce (**42**), Pr (**43**), Nd (**44**), Sm (**45**), Eu (**46**), Tb (**47**), Dy (**48**) and Tm (**49**) [39]. As described above, this series contains a cluster of 18 water molecules, plus six crystallization extra water molecules, that can be easily removed when the samples are heated to 80 °C or simply under vacuum at room temperature (the total number of removed water molecules oscillates between 18 and 22). The removal of the water molecules leads to a colour change of the samples and to an almost complete collapse of the structure, as shown by the X-ray powder diffraction of the evacuated samples (Figure 4a). Studies of the reversibility of this process showed that it is fully reversible and when the dehydrated samples are immersed in water, they recover the original structure (Figure 4a). Moreover, when the dehydrated samples are immersed in different solvents, these solvents enter in the interlayer space and, in some cases, the samples recover the crystallinity, although the new structure is not the same as the hydrated pristine sample (Figure 4b).

Table 3. Ln-anilato compounds with gas/solvent adsorption or solvent exchange capacity.

#	Formula	Ln	Structure	Properties	Reference
35–38 **41–49**	$[Ln_2(dhbq)_3(H_2O)_6]\cdot 18H_2O$	La, Ce, Pr, Nd, Sm, Eu, Gd, Tb, Dy, Ho, Er, Tm, Yb	2D-hexagonal	$-H_2O/+H_2O$ $-H_2O/+$Guess CO_2 adsorption	[39]
58–60 **62,** **64–70**	$[Ln_2(C_6O_4Cl_2)_3(H_2O)_6]\cdot nH_2O$	La, Ce, Pr, Nd, Sm, Eu, Gd, Tb, Dy, Ho, Er	Distorted 2D-hex.	$-H_2O/+H_2O$ $-H_2O/+$Guess CO_2 adsorption	[39]
71–81	$[Ln_2(C_6O_4Br_2)_3(H_2O)_6]\cdot nH_2O$	La, Ce, Pr, Nd, Sm, Eu, Gd, Tb, Dy, Ho, Er	Distorted 2D-hex.	$-H_2O/+H_2O$ $-H_2O/+$Guess CO_2 adsorption	[39]

80	$[Dy_2(C_6O_4Br_2)_3(H_2O)_6]\cdot 8H_2O$	Dy	2D-brickwall	Solv Exch.	[35]
83	$[Dy_2(C_6O_4Br_2)_3(dmso)_6]\cdot 2dmso$	Dy	Distorted 2D-hex.	Solv Exch.	[35]
125	$[Dy_2(C_6O_4Br_2)_3(dmf)_6]$	Dy	2D-herringbone	Solv Exch.	[35]
92	$[La_2(C_6O_4(t\text{-}Bu)_2)_3(dma)_4]$	La	Distorted 2D-hex.	CO_2 abs	[40]
93	$[Pr_2(C_6O_4(t\text{-}Bu)_2)_3(dma)_4]$	Pr	Distorted 2D-hex.	CO_2 abs	[40]
94	$[Nd_2(C_6O_4(t\text{-}Bu)_2)_3(dma)_4]$	Nd	Distorted 2D-hex.	CO_2 abs	[40]
99–100	$[Ln_2(C_6O_4Cl_2)_3(H_2O)_6]\cdot nH_2O$	Tm, Yb	2D-brickwall	$-H_2O/+H_2O$ $-H_2O/+Guess$	[39]
102–103	$[Ln_2(C_6O_4Br_2)_3(H_2O)_6]\cdot nH_2O$	Tm, Yb	2D-brickwall	$-H_2O/+H_2O$ $-H_2O/+Guess$	[39]
131	$(NEt_4)[Y(C_6O_4Cl_2)_2]\cdot 1.4CS_2$	Y	2D-4,4	1.4 CS_2 abs	[41]
132	$(NEt_4)[Y(C_6O_4Cl_2)_2]$	Y	2D-4,4	$N_2/H_2/CO_2/CH_4$	[41]
133	$(NEt_4)[Y(C_6O_4Cl_2)_2]\cdot 1.9I_2$	Y	2D-4,4	1.9 I_2 abs	[41]
134	$(NEt_4)[Y(C_6O_4Cl_2)_2]\cdot 0.9Br_2$	Y	2D-4,4	0.9 Br_2 abs	[41]

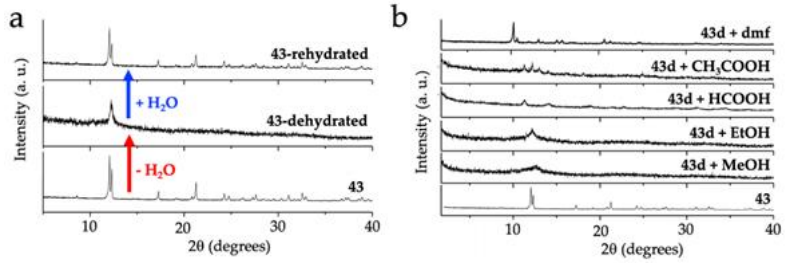

Figure 4. (**a**) X-ray powder diffractogram of compound $(Pr_2(dhbq)_3(H_2O)_6)\cdot 18H_2O$ (**43**), its dehydrated form and the rehydrated one, showing the collapse of the structure upon dehydration and the reversibility of the process. (**b**) X-ray powder diffractogram of compound **43** and the solvated compounds obtained from the dehydrated compound (**43d**) by immersion in different solvents.

The evacuation of the water molecules in compounds **35**-**38** and **41**-**49** leaves empty hexagonal cavities where, besides other solvents, it is also possible to insert gases (Figure 5a). Thus, the dehydrated compounds show CO_2 uptake with a maximum of *ca.* one CO_2 molecule per hexagonal cavity at 0 °C and 100 kPa (Figure 5b).

Similar results have also been observed in the corresponding series with chloranilato, formulated as $[Ln_2(C_6O_4Cl_2)_3(H_2O)_6]\cdot nH_2O$, with Ln(III) = Pr (**58**), Nd (**59**), Tb (**60**), Ce (**61** and **62**), Y (**63**), Gd (**64**), Eu (**65**), Er (**66**), La (**67**), Sm (**68**), Dy (**69**), Ho (**70**), Tm (**99**) and Yb (**100**) [45] and with bromanilato, formulated as $[Ln_2(C_6O_4Br_2)_3(H_2O)_6]\cdot nH_2O$ with Ln/n = La/9 (**72**), Ce/8 (**73**), Pr/11 (**74**), Nd/7 (**75**), Sm/10 (**76**), Eu/6 (**77**), Gd/8 (**78**), Tb/10 (**79**), Dy/8 (**80**), Ho/10 (**81**), Er/7 (**71**), Tm/5.5 (**102**) and Yb/3.5 (**103**). The main difference is that in these two series, the structure does not collapse upon dehydration (only some reflections are lost), probably because now, in contrast with the $dhbq^{2-}$ series, the water molecules do not play any structural role since they are located in the distorted hexagonal or rectangular cavities and in the interlayer space.

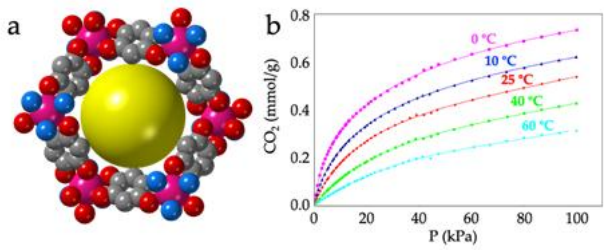

Figure 5. (**a**) View of an empty hexagonal cavity in compounds **35**-**49**. (**b**) Adsorption isothermal for CO_2 uptake at different temperatures for compound **43**.

There are two other very recently published studies showing gas/solvent uptake in Ln-anilato compounds. The first one is a very interesting study performed on compound $(NEt_4)[Y(C_6O_4Cl_2)_2]$ (**132**), a square 2D-4,4 anionic lattice that shows reversible CS_2, I_2 and Br_2 uptake, while keeping the crystallinity [57]. This uptake capacity has allowed the synthesis of compounds $(NEt_4)[Y(C_6O_4Cl_2)_2]\cdot nG$ with nG = 1.43 CS_2 (**131**), 1.87 I_2 (**133**) and 0.91 Br_2 (**134**) . Additionally, compound **132** can also uptake N_2, H_2, CO_2 and CH_4 in its square channels, with high binding enthalpies, among the highest reported for porous coordination polymers, as clearly evidenced by the corresponding adsorption isotherms and by a neutron diffraction study that allowed to determine the location of the adsorbed molecules and their interactions with the lattice.

The second study has been published very recently for compounds $[Ln_2(C_6O_4(t\text{-}Bu)_2)_3(dma)_4]$ with Ln = La (**92**), Pr (**93**) and Nd (**94**). As expected, given the bulky *t*-Bu groups in the anilato ligands, this study has shown a low porosity with CO_2 adsorption isotherms typical of microporous materials.

Finally, we have very recently reported three examples of direct solvent exchange without the need to evacuate the pristine compounds. This study shows that it is possible to exchange the solvent molecules, even the coordinated ones, by immersing compounds $[Dy_2(C_6O_4Br_2)_3(H_2O)_6]\cdot 8H_2O$ (**80**), $[Dy_2(C_6O_4Br_2)_3(dmf)_6]$ (**83**), or $[Dy_2(C_6O_4Br_2)_3(dmso)_4]\cdot 2dmso\cdot 2H_2O$ (**125**) in any of the two other solvents (Figure 6). Interestingly, the three compounds present slow relaxation of the magnetization with different relaxation mechanisms and relaxation times (Table 28) that can be easily modified by simple immersion in the desired solvent.

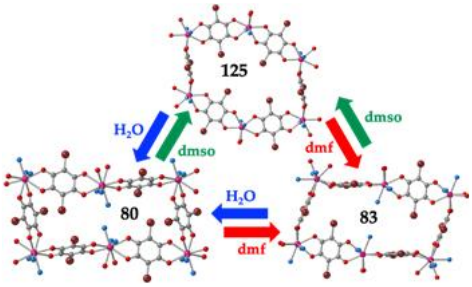

Figure 6. Solvent exchange scheme between compounds $[Dy_2(C_6O_4Br_2)_3(H_2O)_6]\cdot 8H_2O$ (**80**), $[Dy_2(C_6O_4Br_2)_3(dmf)_6]$ (**83**) and $[Dy_2(C_6O_4Br_2)_3(dmso)_4]\cdot 2dmso\cdot 2H_2O$ (**125**).

References

1. Fordham, S.; Wang, X.; Bosch, M.; Zhou, H. Lanthanide Metal-Organic Frameworks: Syntheses, Properties and Potential Applications. Struct. Bond. 2015, 163, 1–27.
2. Wang, C.; Liu, X.; Keser Demir, N.; Chen, J.P.; Li, K. Applications of Water Stable Metal-Organic Frameworks. Chem. Soc. Rev. 2016, 45, 5107–5134.
3. Liu, X.; Fu, W.; Bouwman, E. One-Step Growth of Lanthanoid Metal-Organic Framework (MOF) Films Under Solvothermal Conditions for Temperature Sensing. Chem. Commun. 2016, 52, 6926–6929.
4. Kitagawa, S.; Kawata, S. Coordination Compounds of 1,4-Dihydroxybenzoquinone and its Homologues. Structures and Properties. Coord. Chem. Rev. 2002, 224, 11–34.
5. Benmansour, S.; Vallés-García, C.; Gómez-Claramunt, P.; Mínguez Espallargas, G.; Gómez-García, C.J. 2D and 3D Anilato-Based Heterometallic M(I)M(III) Lattices: The Missing Link. Inorg. Chem. 2015, 54, 5410–5418.
6. Atzori, M.; Benmansour, S.; Mínguez Espallargas, G.; Clemente-León, M.; Abhervé, A.; Gómez-Claramunt, P.; Coronado, E.; Artizzu, F.; Sessini, E.; Deplano, P.; Serpe, A; Mercuri, M. L.; Gómez-García, C.J. A Family of Layered Chiral Porous Magnets Exhibiting Tunable Ordering Temperatures. Inorg. Chem. 2013, 52, 10031–10040.
7. Jeon, I.; Negru, B.; Duyne, R.P.V.; Harris, T.D. A 2D Semiquinone Radical-Containing Microporous Magnet with Solvent-Induced Switching from Tc = 26 to 80 K. J. Am. Chem. Soc. 2015, 137, 15699–15702.
8. Atzori, M.; Artizzu, F.; Sessini, E.; Marchio, L.; Loche, D.; Serpe, A.; Deplano, P.; Concas, G.; Pop, F.; Avarvari, N.; Mercuri, M. L. Halogen-Bonding in a New Family of Tris(Haloanilato)Metallate(III) Magnetic Molecular Building Blocks. Dalt

on Trans. 2014, 43, 7006–7019.

9. Benmansour, S.; Gómez-Claramunt, P.; Vallés-García, C.; Mínguez Espallargas, G.; Gómez García, C.J. Key Role of t he Cation in the Crystallization of Chiral Tris(Anilato)Metalate Magnetic Anions. Cryst. Growth Des. 2016, 16, 518–526.
10. Abrahams, B.F.; Grannas, M.J.; Hudson, T.A.; Hughes, S.A.; Pranoto, N.H.; Robson, R. Synthesis, Structure and Host-Guest Properties of (Et4N)2[SnIVCaII(Chloranilate)4], a New Type of Robust Microporous Coordination Polymer with a 2D Square Grid Structure. Dalton Trans. 2011, 40, 12242–12247.
11. Benmansour, S.; Gómez-García, C.J. A Heterobimetallic Anionic 3,6-Connected 2D Coordination Polymer Based on Nit ranilate as Ligand. Polymers 2016, 8, 89.
12. Kanda, S.; Saito, Y. Synthesis of Co-Ordination Compounds of High Molecular Weight. Bull. Chem. Soc. Jpn. 1957, 30, 192–193.
13. Riley, P.E.; Haddad, S.F.; Raymond, K.N. Preparation of Praseodymium(III) Chloranilate and the Crystal Structures of P r2(C6Cl2O4)3.8C2H5OH and Na3[C6H2O(OH)(SO3)2].H2O. Inorg. Chem. 1983, 22, 3090–3096.
14. Christian, R. Complexes with Substituted 2,5-Dihydroxy-p-Benzoquinones: The Inclusion Compounds [Y(H2O)3]2 (C6 Cl2O4)3•6.6H2O and [Y(H2O)3]2 (C6Br2O4)3•6H2O. Mater. Res. Bull. 1987, 22, 1483–1491.
15. Abrahams, B.F.; Coleiro, J.; Hoskins, B.F.; Robson, R. Gas Hydrate-Like Pentagonal Dodecahedral M2(H2O)18 Cages (M = Lanthanide or Y) in 2,5-Dihydroxybenzoquinone-Derived Coordination Polymers. Chem. Commun. 1996, 603–60 4.
16. Abrahams, B.F.; Coleiro, J.; Ha, K.; Hoskins, B.F.; Orchard, S.D.; Robson, R. Dihydroxybenzoquinone and Chloranilic A cid Derivatives of Rare Earth Metals. J. Chem. Soc. Dalton Trans. 2002, 1586–1594.
17. Mercuri, M.L.; Congiu, F.; Concas, G.; Sahadevan, S.A. Recent Advances on Anilato-Based Molecular Materials with M agnetic and/or Conducting Properties. Magnetochem. 2017, 3, 17.
18. Benmansour, S.; Gómez-García, C.J. Heterometallic Anilato-Based Layered Magnets. Gen. Chem. 2020, 6, 190033.
19. Llunell, M.; Casanova, D.; Cirera, J.; Bofill, J.M.; Alemany, P.; Alvarez, S.; Pinsky, M.; Avnir, D. SHAPE. 2013. v 2.1: htt p://www.ee.ub.edu/index.php?option=com_jdownloads&view=viewcategories&Itemid=529
20. Benmansour, S.; Pérez-Herráez, I.; Cerezo-Navarrete, C.; López-Martínez, G.; Martínez Hernandez, C.; Gómez-Garcí a, C.J. Solvent-Modulation of the Structure and Dimensionality in Lanthanoid-Anilato Coordination Polymers. Dalton Tr ans. 2018, 47, 6729–6741.
21. Ishikawa, R.; Michiwaki, S.; Noda, T.; Katoh, K.; Yamashita, M.; Matsubara, K.; Kawata, S. Field-Induced Slow Magneti c Relaxation of Mono- and Dinuclear Dysprosium(III) Complexes Coordinated by a Chloranilate with Different Resonan ce Forms. Inorganics 2018, 6, 7.
22. Dunstan, M.A.; Rousset, E.; Boulon, M.; Gable, R.W.; Sorace, L.; Boskovic, C. Slow Magnetisation Relaxation in Tetrao xolene-Bridged Rare Earth Complexes. Dalton Trans. 2017, 46, 13756–13767.
23. Zhang, P.; Perfetti, M.; Kern, M.; Hallmen, P.P.; Ungur, L.; Lenz, S.; Ringenberg, M.R.; Frey, W.; Stoll, H.; Rauhut, G.; v an Slageren, J. Exchange Coupling and Single-Molecule Magnetism in Redox-Active Tetraoxolene-Bridged Dilanthanid e Complexes. Chem. Sci. 2018, 9, 1221–1230.
24. Reed, W.R.; Dunstan, M.A.; Gable, R.W.; Phonsri, W.; Murray, K.S.; Mole, R.A.; Boskovic, C. Tetraoxolene-Bridged Rar e-Earth Complexes: A Radical-Bridged Dinuclear Dy Single-Molecule Magnet. Dalton Trans. 2019, 48, 15635–15645.
25. Ishikawa, R.; Michiwaki, S.; Noda, T.; Katoh, K.; Yamashita, M.; Kawata, S. Series of Chloranilate-Bridged Dinuclear La nthanide Complexes: Kramers Systems Showing Field-Induced Slow Magnetic Relaxation. Magnetochem. 2019, 5, 30.
26. Hernández-Paredes, A.; Cerezo-Navarrete, C.; Gómez García, C.J.; Benmansour, S. Slow Relaxation in Doped Coordi nation Polymers and Dimers Based on Lanthanoids and Anilato Ligands. Polyhedron 2019, 170, 476–485.
27. López-Martínez, G. Multifunctionality in Molecular Materials Based on Anilato-Type Ligands. PhD. Thesis. University of Valencia, Valencia, Spain, 2017.
28. Benmansour, S.; Hernández-Paredes, A.; Mondal, A.; López Martínez, G.; Canet-Ferrer, J.; Konar, S.; Gómez-García, C.J. Slow Relaxation of the Magnetization, Reversible Solvent Exchange and Luminescence in 2D Anilato-Based Fram eworks. Chem. Commun. 2020, 56, 9862–9865.
29. Benmansour, S.; Hernández-Paredes, A.; Gómez-García, C.J. Effect of the Lanthanoid-Size on the Structure of a Serie s of Lanthanoid-Anilato 2-D Lattices. J. Coord. Chem. 2018, 71, 845–863.
30. Kingsbury, C.J.; Abrahams, B.F.; Auckett, J.E.; Chevreau, H.; Dharma, A.D.; Duyker, S.; He, Q.; Hua, C.; Hudson, T.A.; Murray, K.S.; Phonsri, W.; Peterson, V. K.; Robson, R.; White, K. F. Square Grid Metal-Chloranilate Networks as Robus t Host Systems for Guest Sorption. Chem. Eur. J. 2019, 25, 5222–5234.
31. Rehwoldt, R.E.; Chasen, B.; Li, J. 2-chloro-5-cyano-3,6-dihydroxybenzoquinone, a New Analytical Reagent for the Spe ctrophotometric Determination of Calcium(II). Anal. Chem. 1966, 38, 1018–1019.
32. Szostak, M.M.; Kozankiewicz, B.; Lipinski, J. Low-Temperature Photoluminescence of p-Nitroaniline and o-Methyl-p-Nit roaniline Crystals. Spectrochim. Acta Part A Mol. Biomol. Spectrosc. 2007, 67, 1412–1416.
33. Atzori, M.; Artizzu, F.; Marchio, L.; Loche, D.; Caneschi, A.; Serpe, A.; Delano, P.; Avarvari, N.; Mercuri, M.L. Switching-on Luminescence in Anilate-Based Molecular Materials. Dalton Trans. 2015, 44, 15786–15802.

34. Bondaruk, K.; Hua, C. Effect of Counterions on the Formation and Structures of Ce(III) and Er(III) Chloranilate Framew orks. Cryst. Growth Des. 2019, 19, 3338–3347.

35. Benmansour, S.; Hernández-Paredes, A.; Gómez-García, C.J. Effect of the Lanthanoid-Size on the Structure of a Serie s of Lanthanoid-Anilato 2-D Lattices. J. Coord. Chem. 2018, 71, 845–863.

36. Kharitonov, A.D.; Trofimova, O.Y.; Meshcheryakova, I.N.; Fukin, G.K.; Khrizanforov, M.N.; Budnikova, Y.H.; Bogomyako v, A.S.; Aysin, R.R.; Kovalenko, K.A.; Piskunov, A.V. 2D-metal–organic Coordination Polymers of Lanthanides (La(III), P r(III) and Nd(III)) with Redox-Active Dioxolene Bridging Ligands. CrystEngComm 2020, 22, 4675–4679.

37. Alvarez, S. Coordinating Ability of Anions, Solvents, Amino Acids and Gases towards Alkaline and Alkaline-Earth Eleme nts, Transition Metals and Lanthanides. Chem. Eur. J. 2020, 26, 8663–8663.

38. Ashoka Sahadevan, S.; Monni, N.; Oggianu, M.; Abhervé, A.; Marongiu, D.; Saba, M.; Mura, A.; Bongiovanni, G.; Mam eli, V.; Cannas, C.; Avarvari, N.; Quochi, F.; Mercuri, M. L. Heteroleptic NIR-Emitting YbIII/Anilate-Based Neutral Coordi nation Polymer Nanosheets for Solvent Sensing. ACS Appl. Nano Mater. 2020, 3, 94–104.

39. Benmansour, S.; Pérez-Herráez, I.; López-Martínez, G.; Gómez García, C.J. Solvent-Modulated Structures in Anilato-B ased 2D Coordination Polymers. Polyhedron 2017, 135, 17–25.

40. Ishikawa, R.; Michiwaki, S.; Noda, T.; Katoh, K.; Yamashita, M.; Kawata, S. Series of Chloranilate-Bridged Dinuclear La nthanide Complexes: Kramers Systems Showing Field-Induced Slow Magnetic Relaxation. Magnetochem. 2019, 5, 30.

41. Kingsbury, C.J.; Abrahams, B.F.; Auckett, J.E.; Chevreau, H.; Dharma, A.D.; Duyker, S.; He, Q.; Hua, C.; Hudson, T.A.; Murray, K.S.; Phonsri, W.; Peterson, V. K.; Robson, R.; White, K. F. Square Grid Metal-Chloranilate Networks as Robus t Host Systems for Guest Sorption. Chem. Eur. J. 2019, 25, 5222–5234.

42. Benmansour, S.; Hernández-Paredes, A.; Gómez-García, C.J. Two-Dimensional Magnetic Coordination Polymers For med by Lanthanoids and Chlorocyananilato. Magnetochem. 2018, 4, 58.

43. Ashoka Sahadevan, S.; Monni, N.; Abhervé, A.; Marongiu, D.; Sarritzu, V.; Sestu, N.; Saba, M.; Mura, A.; Bongiovanni, G.; Cannas, C.; Quochi, F.; Avarvari, N.; Mercuri, M. L. Nanosheets of Two-Dimensional Neutral Coordination Polymers Based on Near-Infrared-Emitting Lanthanides and a Chlorocyananilate Ligand. Chem. Mater. 2018, 30, 6575–6586.

44. Zucchi, G.; Thuery, P.; Ephritikhine, M.; CSD Communication, 2012.

45. Benmansour, S.; Pérez-Herráez, I.; López-Martínez, G.; Gómez García, C.J. Solvent-Modulated Structures in Anilato-B ased 2D Coordination Polymers. Polyhedron 2017, 135, 17–25.

46. Kharitonov, A.D.; Trofimova, O.Y.; Meshcheryakova, I.N.; Fukin, G.K.; Khrizanforov, M.N.; Budnikova, Y.H.; Bogomyako v, A.S.; Aysin, R.R.; Kovalenko, K.A.; Piskunov, A.V. 2D-metal–organic Coordination Polymers of Lanthanides (La(III), P r(III) and Nd(III)) with Redox-Active Dioxolene Bridging Ligands. CrystEngComm 2020, 22, 4675–4679.

47. Demars, T.; Boltoeva, M.; Vigier, N.; Maynadié, J.; Ravaux, J.; Genre, C.; Meyer, D. From Coordination Polymers to Do ped Rare-Earth Oxides. Eur. J. Inorg. Chem. 2012, 2012, 3875–3884.

48. Bondaruk, K.; Hua, C. Effect of Counterions on the Formation and Structures of Ce(III) and Er(III) Chloranilate Framew orks. Cryst. Growth Des. 2019, 19, 3338–3347.

49. Dunstan, M.A.; Rousset, E.; Boulon, M.; Gable, R.W.; Sorace, L.; Boskovic, C. Slow Magnetisation Relaxation in Tetrao xolene-Bridged Rare Earth Complexes. Dalton Trans. 2017, 46, 13756–13767.

50. Zhang, P.; Perfetti, M.; Kern, M.; Hallmen, P.P.; Ungur, L.; Lenz, S.; Ringenberg, M.R.; Frey, W.; Stoll, H.; Rauhut, G.; v an Slageren, J. Exchange Coupling and Single-Molecule Magnetism in Redox-Active Tetraoxolene-Bridged Dilanthanid e Complexes. Chem. Sci. 2018, 9, 1221–1230.

51. Reed, W.R.; Dunstan, M.A.; Gable, R.W.; Phonsri, W.; Murray, K.S.; Mole, R.A.; Boskovic, C. Tetraoxolene-Bridged Rar e-Earth Complexes: A Radical-Bridged Dinuclear Dy Single-Molecule Magnet. Dalton Trans. 2019, 48, 15635–15645.

52. Ishikawa, R.; Michiwaki, S.; Noda, T.; Katoh, K.; Yamashita, M.; Kawata, S. Series of Chloranilate-Bridged Dinuclear La nthanide Complexes: Kramers Systems Showing Field-Induced Slow Magnetic Relaxation. Magnetochem. 2019, 5, 30.

53. Hernández-Paredes, A.; Cerezo-Navarrete, C.; Gómez García, C.J.; Benmansour, S. Slow Relaxation in Doped Coordi nation Polymers and Dimers Based on Lanthanoids and Anilato Ligands. Polyhedron 2019, 170, 476–485.

54. Benmansour, S.; Hernández-Paredes, A.; Mondal, A.; López Martínez, G.; Canet-Ferrer, J.; Konar, S.; Gómez-García, C.J. Slow Relaxation of the Magnetization, Reversible Solvent Exchange and Luminescence in 2D Anilato-Based Fram eworks. Chem. Commun. 2020, 56, 9862–9865.

55. Benmansour, S.; Hernández-Paredes, A.; Gómez-García, C.J. Effect of the Lanthanoid-Size on the Structure of a Serie s of Lanthanoid-Anilato 2-D Lattices. J. Coord. Chem. 2018, 71, 845–863.

56. Kingsbury, C.J.; Abrahams, B.F.; Auckett, J.E.; Chevreau, H.; Dharma, A.D.; Duyker, S.; He, Q.; Hua, C.; Hudson, T.A.; Murray, K.S.; Phonsri, W.; Peterson, V. K.; Robson, R.; White, K. F. Square Grid Metal-Chloranilate Networks as Robus t Host Systems for Guest Sorption. Chem. Eur. J. 2019, 25, 5222–5234.

57. Rehwoldt, R.E.; Chasen, B.; Li, J. 2-chloro-5-cyano-3,6-dihydroxybenzoquinone, a New Analytical Reagent for the Spe ctrophotometric Determination of Calcium(II). Anal. Chem. 1966, 38, 1018–1019.

58. Szostak, M.M.; Kozankiewicz, B.; Lipinski, J. Low-Temperature Photoluminescence of p-Nitroaniline and o-Methyl-p-Nit roaniline Crystals. Spectrochim. Acta Part A Mol. Biomol. Spectrosc. 2007, 67, 1412–1416.

59. Atzori, M.; Artizzu, F.; Marchio, L.; Loche, D.; Caneschi, A.; Serpe, A.; Delano, P.; Avarvari, N.; Mercuri, M.L. Switching-on Luminescence in Anilate-Based Molecular Materials. Dalton Trans. 2015, 44, 15786–15802.
60. Ashoka Sahadevan, S.; Monni, N.; Oggianu, M.; Abhervé, A.; Marongiu, D.; Saba, M.; Mura, A.; Bongiovanni, G.; Mameli, V.; Cannas, C.; Avarvari, N.; Quochi, F.; Mercuri, M. L. Heteroleptic NIR-Emitting YbIII/Anilate-Based Neutral Coordination Polymer Nanosheets for Solvent Sensing. ACS Appl. Nano Mater. 2020, 3, 94–104.